602879

The force exerted by the membrane potential during protein import into the mitochondrial matrix

Karim Shariff * Sandip Ghosal † Andreas Matouschek ‡

August 1, 2002

Abstract

The electrostatic force exerted on a targeting sequence by the electrical potential across the inner mitochondrial membrane is calculated and found to vary from 1.4 pN to 2.2 pN (per unit elementary charge) as the radius of the inner membrane pore (assumed aqueous) is varied from 12 to 6.5 Å, its measured range. Since the pore is not very much wider than the distance between water molecules, the full shielding effect of water may not be present; the extreme case of a non-aqueous pore gives a force of 3.1 pN per unit charge, which represents an upper limit. When applied to mitochondrial import experiments on the protein barnase, these results imply that a force of 11 ± 4 pN is sufficient to catalyze the unfolding of barnase during import. Comparison of these results with unfolding forces measured using atomic force microscopy suggests that the two are not inconsistent.

1 Introduction

Most mitochondrial proteins are encoded in the cell's nuclear DNA, manufactured within the cytosol as precursors, and translocated into mitochondria across the organelle's inner and outer membranes (henceforth IM and OM) through points where the two membranes come into contact. For the basic facts consult Alberts et al. (1994) and Pfanner and Neupert (1990). After translocation, the precursors are sent to the appropriate mitochondrial subcompartment where they are assembled into protein complexes. Most precursors that are targeted to the lumen of the mitochondria, called the matrix, are synthesized with a targeting sequence (TS), also called a presequence, attached at their amino terminus. This TS marks the precursor for translocation. We are concerned with precursors that are folded prior to import and where the TS protrudes from the precursor. Targeting sequences of this kind always have an abundant number of positively charged residues with few negative ones. As previously suggested (e.g , Martin, Mahlke, and Pfanner, 1991) the positive charges allow the inner membrane's electric potential to exert a force that is directed into the mitochondrion.

The translocation of protein precursors into mitochondria involve a number of actors (Pfanner and Truscott, 2002) besides the membrane potential; see Fig. 1. The TS first interacts with protein receptors (Tom20 and Tom22) on the surface of the outer membrane. These receptors may promote insertion of the TS into the OM pore, which itself consists of the protein Tom40. The pore of the inner membrane likewise consists of transmembrane proteins (Tim17 and Tim23). A portion of the Tim23 protein that lies exposed on the outer face of the IM appears to facilitate insertion of the TS into the IM pore; the membrane potential activates the insertion (Bauer et al., 1996). The passage of the TS through the IM pore may be driven by thermal motion, the electric field of the membrane potential, interaction with the Tim proteins, or a combination.

*NASA Ames Research Center, Moffett Field, CA 94035
†Department of Mechanical Engineering, Northwestern University, Evanston, IL 60208
‡Department of Biochemistry, Molecular Biology and Cell Biology, Northwestern University, Evanston, IL 60208

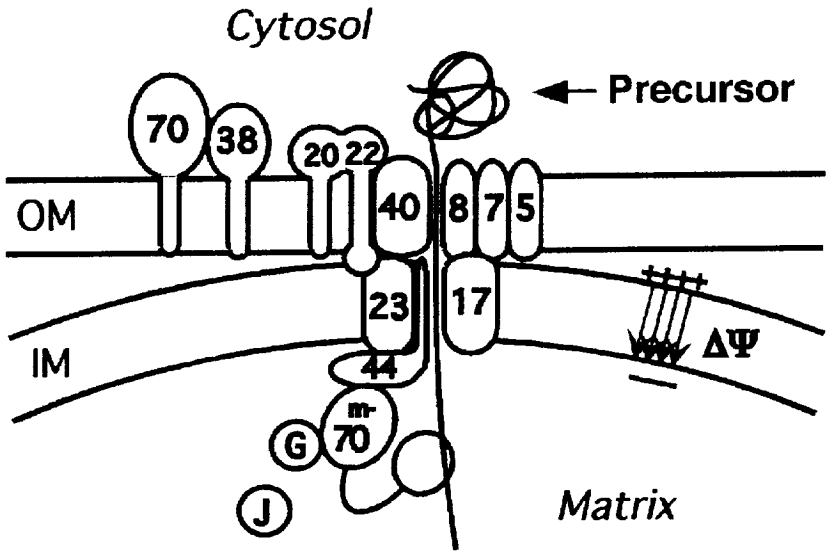

Figure 1: Schematic of protein import.

Once the TS has been threaded into both OM and IM pores, the bulk of the protein lying on the outer mitochondrial surface must then unfold. Huang et al. (1999) concluded that the unfolding is initiated at the targeting sequence and that precursor proteins are unraveled sequentially from their N-termini. The unraveling occurs when the targeting sequence engages the unfolding machinery associated with the inner mitochondrial membrane while the structured domain remains at the entrance to the import channel. The simplest mechanism by which the import machinery could unravel a protein at a distance would be by pulling at the targeting sequence. Atomic force microscopy (AFM) experiments show that the N-terminus of a protein needs to be pulled only a short distance before the protein denatures. This distance is an empirically defined width of the potential well for unfolding and its values range between 3 and 17 Å for different domains (Rief et al., 1997; Rief et al., 1998; Best et al., 2001).

What pulls the targeting sequence through the required distance? If the TS is long enough to span both membranes and reach sufficiently far into the mitochondrial matrix, then Tim44 in association with mtHsp70 is able to unfold the protein by an ATP driven action (e.g., Matouschek, Pfanner, and Voos, 2000). Many targeting sequences, however, are not long enough to span both membranes; for instance the total thickness of yeast mitochondrial membranes is at least ≈ 140 Å. This corresponds to 40 amino acids in the fully extended conformation while the average length of yeast presequences is smaller, viz, 31 amino acids (Huang, Ratliff, and Matouschek, 2002). When targeting sequences are not long enough to interact with mtHsp70, the rate of import of precursor proteins depends upon the strength of the electrical potential and the number of positively charged amino acids (Huang, Ratliff, and Matouschek, 2002). The simplest implication of this result is that for short targeting sequences, the force exerted by the inner membrane potential upon the charged residues of the targeting sequence unfolds the passenger protein. In this work we investigate this hypothesis by calculating the electrostatic force exerted by the potential and make a preliminary attempt to determine whether it is sufficient to unravel a protein.

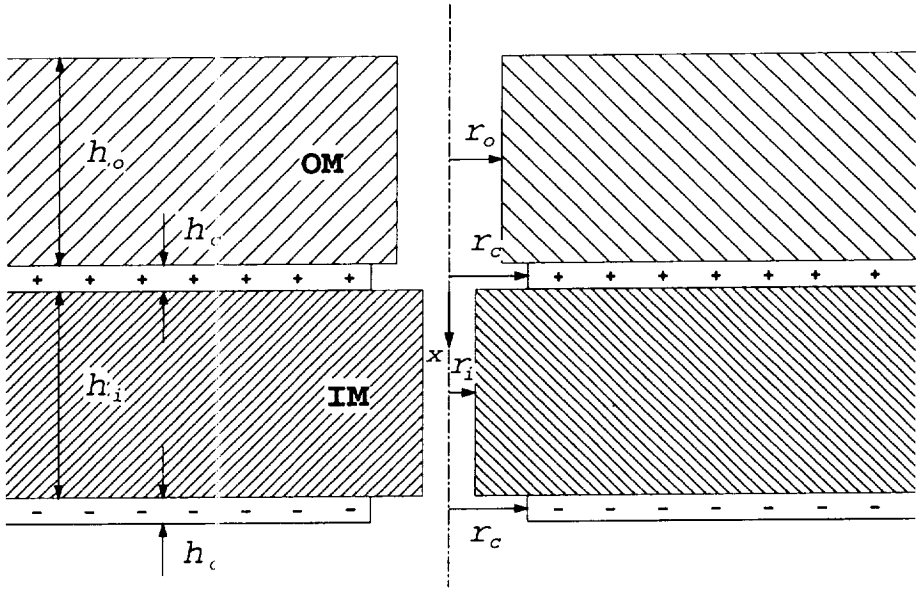

Figure 2: Sketch for computational model. Subscripts: o, outer membrane; i, inner membrane; c, charge layer.

2 Model

2.1 Computational Model

A distribution of charge density $\rho(\mathbf{x})$ (per unit volume) in a medium with dielectric constant $\epsilon(\mathbf{x})$ produces an electric field $\mathbf{E} = -\nabla\phi$, where ϕ is obtained from

$$\nabla \cdot (\epsilon \nabla \phi) = -4\pi\rho. \tag{1}$$

Fig. 2 shows the geometry assumed for the distributions of $\epsilon(\mathbf{x})$ and $\rho(\mathbf{x})$. Shading denotes membraneous regions where $\epsilon = 1$. Lack of shading denotes aqueous regions ($\epsilon = 80$). These include the cytosol, mitochondrial matrix, and the intermembrane space where the layer of + charge is located. The dielectric constant incorporates the shielding of charges by water dipoles. There is also screening by ions; at pH near 7, however, the Debye shielding distance (e.g., Probstein, 1994) is about 1 μm, rendering this effect negligible at the length scales of present interest.

The OM and IM pores are also assumed to be aqueous based on their observed hydrophilic character (see Hill et al., 1998; Truscott et al., 2001). The radius r_o of the OM pore was taken to be 12 Å based on reported measurements, namely, between 10 and 13 Å according to Schwartz and Matouschek (1999), 11 Å according to Hill et al. (1998), and 10 Å according to Künkele et al. (1998). Less is known about the radius r_i of the IM pore. Schwartz and Matouschek (1999) concluded that r_i is at most 10 Å. Here we will consider values in the wider range $6.5 < r_i < 12$ Å, suggested by Truscott et al. (2001). Since the spacing between water molecules is about 3 Å, only a few water molecules will be able to occupy the pores. To qualitatively allow for such an effect, values of r_i down to 0 Å, representative of a non-dielectric pore, will also be considered.

For the value of the mitochondrial membrane potential, $\Delta\Psi$, we used 150 mV corresponding to the protein import experiments of Huang, Ratliff, and Matouschek (2002). The charge density σ

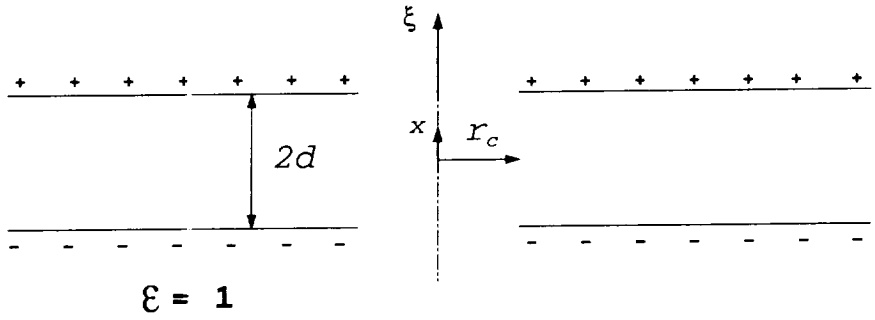

Figure 3: Sketch for analytical model.

(per unit area) is then inferred to be

$$\sigma = \frac{\Delta\Psi}{4\pi(2d)}, \tag{2}$$

where $2d = h_i + h_c$ is the distance between the charged layers. The volume charge density is then $\rho = \sigma/h_c$

We took $h_i = h_o = 65$ Å, a value consistent with electron micrograph pictures. The radius r_c of the holes in the charged layers was taken to be 10 Å. The thickness of charge layers $h_c = 10$ Å, a reasonable guess; the electric field away from the edges of the charge layers will be insensitive to h_c.

Equation 1 was solved numerically using a B-spline Galerkin scheme (Shariff and Moser, 1998) in cylindrical polar coordinates (x, r), where x is the axial coordinate (measured from the entrance of the IM pore and positive into the mitochondrion) and r is the radius. The discretization cells were designed to be small at interfaces where jumps in dielectric constant and charge density occur, and to become larger as the computational boundary is approached. In most runs the smallest computational cell size was 1Å × 1Å and the computational domain was $x \in [-200, 200]$Å, $r \in [0, 110]$Å. As a check on accuracy, a computation with half the cell sizes in each direction and twice the radial domain size was also run. The boundary condition $\partial\phi/\partial n = 0$ was applied at the boundary of the computational domain which is large enough for the boundary condition to be accurate. Here n is the coordinate normal to the boundary. At the symmetry axis we also required $\partial\phi/\partial r = 0$ which is precisely the condition required for an axisymmetric function to have continuous radial derivatives at the axis. Since the Galerkin method is based upon integrals, discontinuous distributions of $\epsilon(\mathbf{x})$ and $\rho(\mathbf{x})$, which occur in the present model, can be treated. At an interface across which ϵ suffers a jump, E_n, the component of the electric field normal to the interface also jumps. Since the computed solution is a projection of the exact solution upon the space of B-splines, this jump leads to some Gibbs oscillation in E_n. Such oscillation may be witnessed in Fig. 5 and was generally found to be weak.

2.2 Analytical Model

Since $\nabla \times \mathbf{E} = 0$, the tangential component of $\mathbf{E}$ is always continuous across charge layers and across discontinuities in ϵ; since $\nabla \cdot (\epsilon\mathbf{E}) = 0$ outside of charge layers, the normal component of $\mathbf{E}$ suffers a jump across discontinuities in ϵ (see e.g., Jackson, 1962, Ch. 1). In particular, when ϵ increases by a factor of 80 across an interface, the component of the electric field normal to the interface diminishes by the same factor.

For the case of a thin pore ($r_i \ll h_i$ and $r_o \ll h_o$, which is typical), we expect that the electric field in the membrane space, will be primarily in the axial (x) direction, and will therefore persist in the aqueous pore without being substantially diminished by the presence of water. Hence, as an

approximation we take $\epsilon = 1$ everywhere. In addition we take the charge layers to be infinitesimally thin plates (Fig. 3).

In this sub-section, let the positive axial direction (ξ) point out of the mitochondrion. Let $\widetilde{E}(\xi)$ denote the axial (ξ) component of the electric field due to a single plate with a hole (at $\xi = 0$) of radius r_c and surface charge density σ. We are evaluating the electric field along the axis of the hole ($r = 0$) where only the axial component is non-zero. Let $E'(\xi)$ denote the axial electric field of the charged disk which closes the hole. Then,

$$\widetilde{E}(\xi) + E'(\xi) = 2\pi\sigma, \tag{3}$$

the right-hand side being the electric field of an infinite plate. Integrating the inverse square law over the disk gives

$$E'(\xi) = \sigma \int_0^{r_c} \int_0^{2\pi} \frac{r d\varphi\, dr}{(r^2 + x^2)} \cos\theta, \tag{4}$$

where $\cos\theta = \xi/\sqrt{\xi^2 + r^2}$. Carrying out the integration in (4) and using (3) gives

$$\widetilde{E}(\xi;\sigma) = \frac{2\pi\sigma\xi}{\sqrt{{r_c}^2 + \xi^2}}. \tag{5}$$

Finally, superposing two plates spaced a distance $2d$ apart we have:

$$E(x) = \widetilde{E}(x - d;\sigma) + \widetilde{E}(x + d;-\sigma), \tag{6}$$

where x is measured from the midpoint of the two charged layers (see Fig. 3). The peak value of the field occurs at $x = 0$ and is:

$$E_{\text{peak}} = -\frac{4\pi\sigma d}{\sqrt{{r_c}^2 + d^2}}. \tag{7}$$

In the limit $r_c \ll d$ we get:

$$E_{\text{peak}} = -4\pi\sigma = -\frac{\Delta\Psi}{2d}, \tag{8}$$

the electric field in a parallel plate capacitor. The corresponding axial force $F_{e,\text{peak}} = eE_{\text{peak}}$ per unit (+) elementary charge (e) is

$$F_{e,\text{peak}}(\text{pN}) = -1.6\frac{\Delta\Psi(\text{mV})}{2d(\text{Å})}, \tag{9}$$

in the ξ direction. Equation 9 is a convenient formula for calculating an upper limit on the force.

3 Results and Discussion

Fig. 4 is a result of the computational model. It shows the force field exerted on a particle having a charge equal to that of the electron but with a positive sign. Colors depict the magnitude of the force and the arrows provide its direction. The force within the IM pore is remarkably uniform, both radially and axially. Whatever leakage there is of the field at the entrance of the IM pore has a direction that is favorable to centering and insertion of the targeting sequence into pore. The field direction at the exit of the IM pore is favorable for diffusion and exit out of the pore.

The radial uniformity of the force field within the pore ($r < r_i = 6.5$ Å here) is illustrated in Fig. 5. At the pore boundary ($r = 6.5$ Å) the force field suffers a jump in derivative and then at large distances from the pore relaxes slowly to the uniform field of a parallel plate capacitor.

Fig. 6 plots the force along the axis of the pores for various values of the radius of the IM pore. As the radius, r_i, of the IM pore decreases, the electric field increases as a result of less shielding by

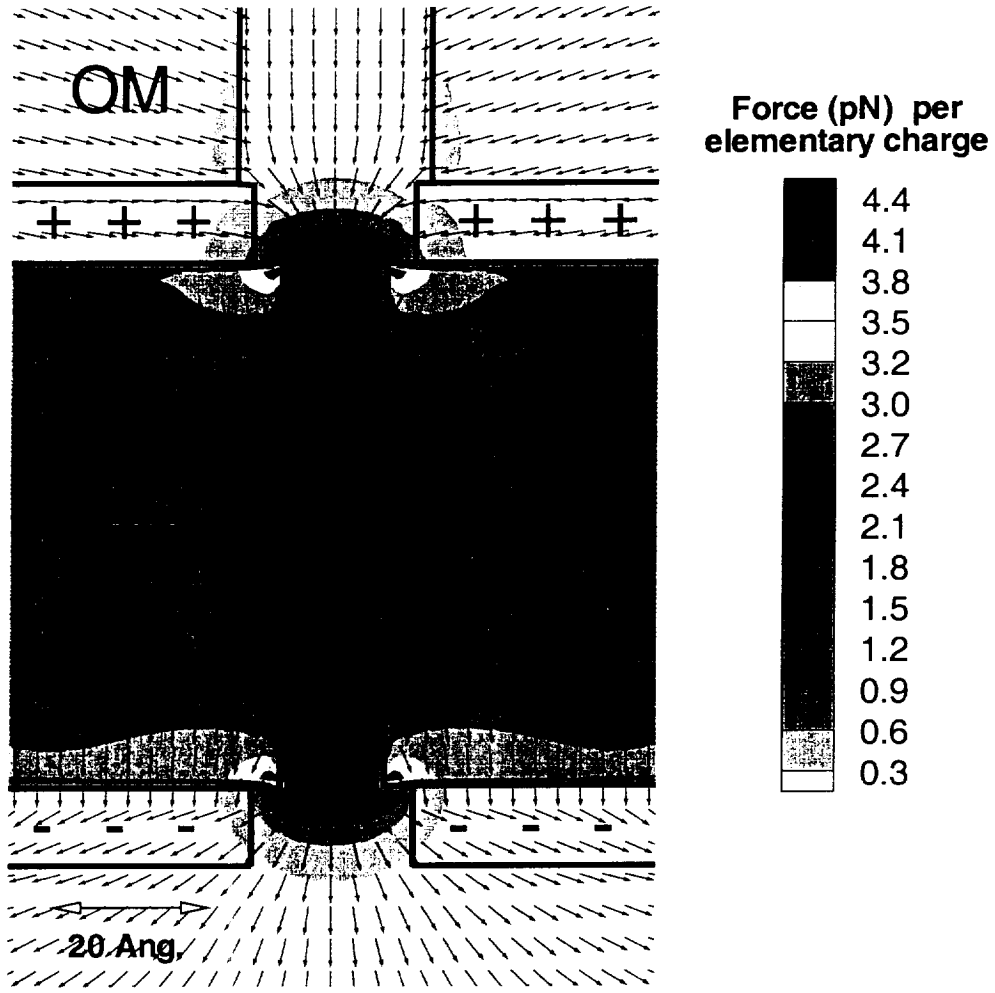

Figure 4: Electrostatic force per elementary (+) charge. The radius, r_i of the IM pore is 6.5 Å here. Colors depict the magnitude of the force while arrows show its direction.

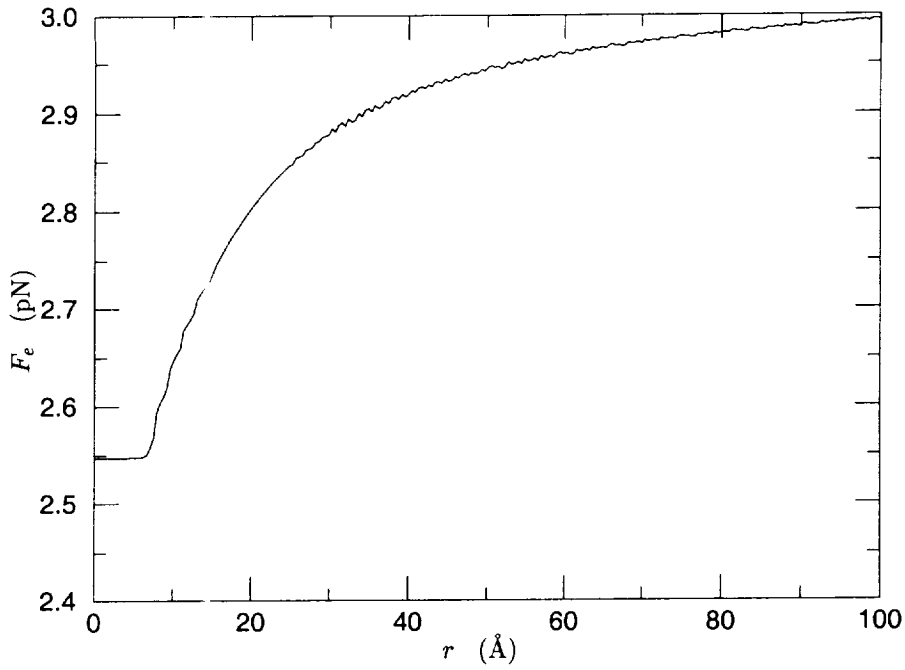

Figure 5: Radial profile of the force per elementary charge for the case of $r_i = 6.5$ Å. The profile is taken at the mid-section of the pore. The small oscillation is Gibbs phenomenon, an artifact of the numerical solution.

water. The result (solid line) of the analytical model (6) provides an upper bound and becomes a better approximation to the results of the computational model as the pore radius diminishes. The force profile given by the computational model is quite uniformly distributed along the pore and indicates a small leakage of the electric field into the OM pore. If we let the radius of the IM pore take on values ranging from 0 Å (to allow for the possibility of a completely non-dielectric pore) up to 12 Å, then we conclude that $1.4 < F_{e,\text{peak}} < 3.1$ pN.

Next, consider import experiments for the protein barnase (Huang, Ratliff, and Matouschek, 2002) and focus on those cases in which the unfolding mode ranges from being spontaneous to membrane potential driven (see Table 1), i.e., exclude cases for long presequences which are unfolded by mtHsp70. The column in Table 1 labeled "Unfolding mode" gives a qualitative indication of the relative importance of spontaneous (denoted S) and membrane potential (denoted M) driven unfolding in each experiment. The net number of positive charges is determined as described in the

Targeting Sequence	Net no. of + charges in IM pore	Total force (pN)	Import rate (Å s^{-1})	Unfolding mode
(35)	3	4.2–9.3	$0.35 \pm .02$	SSSS
(35; A16K)	4	5.6–12.4	$0.53 \pm .04$	SSMM
(35+5)	4	5.6–12.4	$0.87 \pm .09$	SSMM
(65)	0–3	0.0–9.3	$1.3 \pm .2$	SMMM
(35; E15L)	5	7.0–15.5	$2.4 \pm .1$	MMMM

Table 1: Predicted forces for mitochondrial import experiments (Huang, Ratliff, and Matouschek, 2002)

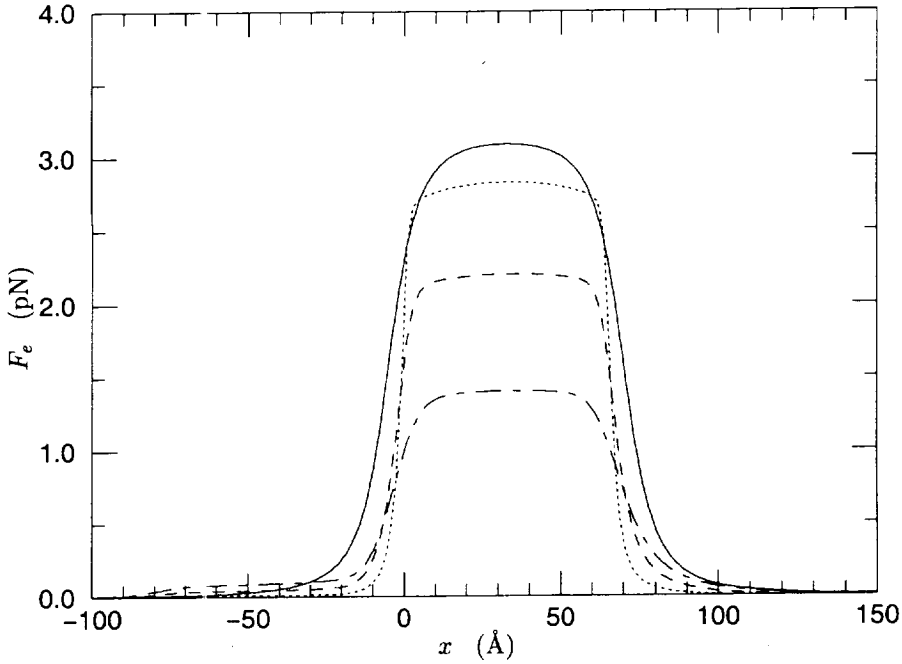

Figure 6: Force per elementary (+) charge. The origin of the abscissa lies at the entrance of the IM pore which is 65 Å long. Positive force is directed into the mitochondrion. ——— : using the analytical result (6); computational results: ····· , $r_i = 3$ Å; ---- , $r_i = 6.5$ Å; —·— , $r_i = 12$ Å.

appendix and after multiplication by the range of F_e in the previous paragraph, we obtain the values in the "Total Force" column. One observes a trend, more or less, of increasing import rate with increasing predicted force; the case of targeting sequence (65) is anomalous. Import with the (35; E15L) presequence is, by all indications of the experiment, catalyzed by the membrane potential; the force that accomplishes this lies between 7 and 15.5 pN.

Are these forces consistent with atomic force microscopy (AFM) experiments for barnase (Best et al., 2001)? First, let us caution that pulling a protein during mitochondrial import could be different than during AFM experiments which pull free proteins in solution. One mechanism for the difference is a drag force (Chauwin, Oster, and Glick, 1998). Another difference is that in AFM the displacement is imposed whereas during import the force is imposed.

Best et al. (2001) conducted AFM pulling experiments on tandem repeats of barnase followed by the titin domain I27, and they extracted unfolding forces for the barnase units alone. Their data (circles) are plotted in Fig. 7 along side the data (error bars) of Table 1. The dependence of pulling rate k_p on applied force F in the many AFM experiments to date follows Bell's law (Evans and Ritchie, 1999):

$$k_\mathrm{p} = k_\mathrm{p}^0 e^{F\Delta x_\mathrm{u}/kT}, \tag{10}$$

where kT is the product of Boltzmann's constant and temperature, k_p^0 and Δx_u are constants fit to the data. The quantity Δx_u has the interpretation of a potential-well-width for unfolding. Bell's law plots as a straight line in a semi-log graph like figrefBest. In their experiments on the unfolding of titin domains, Carrion-Vasquez et al. (1999) observed that the zero force extrapolation (using Bell's law) of their AFM rates coincided with the zero denaturant extrapolation of chemical denaturation rates obtained for isolated domains of titin. This result suggests that extrapolation of the AFM data to smaller forces using Bell's law might be valid. If the presently predicted forces are consistent with

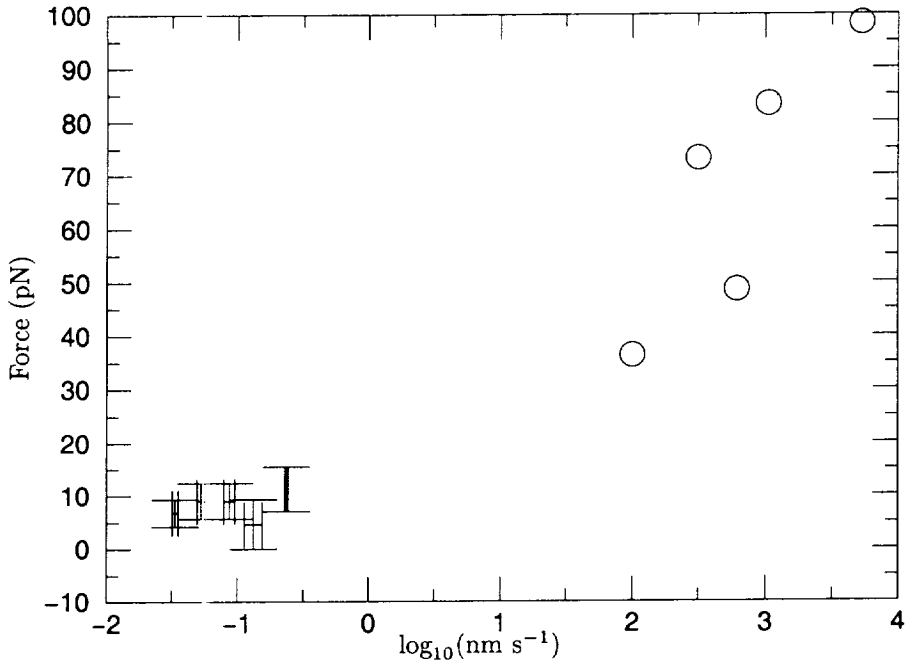

Figure 7: Force vs. rate of pulling (AFM) or rate of import. o : AFM experiments (Best et al., 2001); error bars: protein import data from Table 1. The five error bars from left to right correspond sequentially to the entries in Table 1

forces measured in the barnase AFM experiment, and both are consistent with the same Bell's law, they should lie on the same line in Fig. 7. This is difficult to conclude given the scatter in the data. All we can say at present is that the two are not inconsistent. Of course, this is not saying a whole lot given that a prediction of zero force would also appear to not be inconsistent when plotted on Fig. 7.

A Net number of positive charges within the IM pore

The net number of positive charges lying within the IM pore of the experiment (Huang, Ratliff, and Matouschek, 2002) is inferred as follows. First, from the pH of the experiment (= 7.4), we determined (from the Henderson-Hasselbach equation) that the ionization fraction is .998 or better for all the acidic and basic amino acids in the presequence. Since the pK of the N-terminus is uncertain ($6.8 < pK < 8$), its ionized fraction could range from .2 to .8 (with a positive charge); for simplicity we considered it as uncharged. For presequence (35), the experiment reported membrane potential catalyzed unfolding when positive charges were introduced at positions 15 or 16 but not when they were introduced at positions 18 or 19. Hence the last residue lying within the IM pore is either 16 or 17. Examination of the amino acid sequence then gives 3 net positive charges as lying within the IM pore. The number of charges for presequences (35; A16K) and (35; E15L) then follows naturally. Presequence (35+5) allows five more residues to occupy the IM pore and these add one more positive charge. The presequence (65) will have positions 46 or 47 (30 + either 16 or 17) as the last one lying in the IM pore. These consist of 6 or 7 net positive charges. However, taking the length of the IM pore to be between 65 and 90 Å, we infer that between 20 and 28 amino acids (consisting of 4 to 6 net positive charges) will stick out at the matrix end of the IM pore. Hence we

have between 0 and 3 (6 to 7 minus 4 to 6) net positive charges.

A.M. was supported by NIH grant R01GM63004.

References

[1] Alberts, B., Bray, D., Lewis, J., Raff, M., Roberts, K., and J.D. Watson. 1994. *Molecular Biology of the Cell.* Garland Publishing.

[2] Bauer, M.F., Sirrenberg, C., Neupert, W. and M. Brunner. 1996. Role of Tim23 as voltage sensor and presequence receptor in protein import into mitochondria. *Cell* 87:33–41.

[3] Best, R.B., Li, B., Steward, A., Daggett, V. and J. Clarke. 2001. Can non-mechanical proteins withstand force? Stretching barnase by atomic force microscopy and molecular dynamic simulation. *Biophys. J.* 81:2344–2356.

[4] Carrion-Vasquez, M., Oberhauser, A.F., Fowler, S.B., Marszalek, P.E., Broedel, S.E., Clarke, J. and J.M. Fernandez. 1999. Mechanical and chemical unfolding of a single protein: A comparison. *Proc. Natl. Acad. Sci. USA*, 96:3694–3699.

[5] Chauwin, J.-F., Oster, G. and B.S. Glick. 1998. Strong precursor-pore interactions constrain models for mitochondrial protein import. *Biophys. J.* 74:1732–1743.

[6] Hill, H., Model, K., Ryan, M.T., Dietmeier, K., Martin, F., Wagner, R., and N. Pfanner. 1998. Tom40 forms the hydrophilic channel of the mitochondrial import pore for preproteins. *Nature* 395:516–521.

[7] Huang, S., Ratliff, K.S., Schwartz, M.P., Spenner, J.M., and A. Matouschek. 1999. Mitochondria unfold precursor proteins by unraveling them from their N-termini. *Nature Struct. Biol.* 6:1132–1138.

[8] Huang, S., Ratliff, K.S., and A. Matouschek. 2002. Protein unfolding by the mitochondrial membrane potential. *Nature Struct. Biol.* 9:301–307.

[9] Jackson, J.D. 1962. *Classical Electrodynamics.* Wiley.

[10] Evans, E. and K. Ritchie. 1999. Strength of a weak bond connecting flexible polymer chains. *Biophys. J.* 76:2439–2447

[11] Künkele, K.-P., Heins, S., Dembowski, M., Nargang, F.E., Benz, R., Thieffry, M., Walz, J., Lill, R., Nussberger, S., and W. Neupert. 1998. The preprotein translocation channel of the outer membrane of mitochondria. *Cell*, 93:1009–1019.

[12] Li, H., Oberhauser, A.F., Fowler, S.B., Clarke, and J.M. Fernandez. 2000. Atomic force microscopy reveals the mechanical design of a modular protein. *Proc. Nat. Acad. Sci. USA* 97:6527–6531.

[13] Martin, J., Mahlke, K., and N. Pfanner. 1991. Role of an energized inner membrane in mitochondrial protein import: $\Delta\Psi$ drives the movement of presequences. *J. Biol. Chem.* 266:18051–18057.

[14] Matouschek, A., Pfanner, N., and W. Voos. 2000 Protein unfolding by mitochondria: The Hsp70 import motor. EMBO *Reports*, 1:404–410.

[15] Pfanner, N. and W. Neupert. 1990. The mitochondrial protein import apparatus. *Ann. Rev. Biochem.* 59:331–353.

[16] Pfanner, N. and K.N. Truscott. 2002. Powering mitochondrial protein import. *Nature Struct. Bio.* 9:234–236.

[17] Probstein, R.F. 1994. *Physico-Chemical Hydrodynamics.* Wiley-Interscience.

[18] Rief, M., Pascual, J., Saraste, M., and H.E. Gaub. 1998. Single molecule force spectroscopy of spectrin repeats: low unfolding forces in helix bubdles. *J. Mol. Biol.* 286:553–561.

[19] Rief, M., Gautel, M., Oesterhelt, F., Fernandez, J.M., and H.E. Gaub. 1997. Reversible unfolding of individual titin immunoglobulin domains by AFM. *Science*, 276:1109–1112.

[20] Schwartz, M.P. and A. Matouschek. 1999. The dimensions of the protein import channels in the outer and inner mitochondrial membranes. *Proc. Nat. Acad. Sci. USA* 96:13086–13090.

[21] Shariff, K. and R.D. Moser. 1998. Two-dimensional mesh embedding for B-spline methods. *J. Comp. Phys.* 145:471–488.

[22] Truscott, K.N., Kovermann, P., Geissler, A., Merlin, A., Meijer, M., Driessen, A.J.M., Rassow, J., Pfanner, N., and R. Wagner. 2001. A presequence- and voltage-sensitive channel of the mitochondrial preprotein translocase formed by Tim23. *Nature Struct. Bio.* 8:1074–1082.